

Longitudinal single-cell analysis reveals RUNX1T1 as an early driver in treatment-induced neuroendocrine transdifferentiation

Yuchao Ni^{1,2,5,6}, Dong Lin^{1,2,6}, Mingchen Shi^{1,2,6}, Yen-Yi Lin^{1,2,6}, Hui Xue³, Xin Dong³, Liangliang Liu^{1,2}, Funda Sar^{1,2}, Rebecca Wu³, Tunc Morova^{1,2}, Anne Haegert^{1,2}, Robert Bell^{1,2}, Xinyao Pang^{1,2}, Adam Classen^{2,3}, Yu Wang^{1,2}, Junru Chen⁵, Stanislav Volik^{1,2}, Stéphane Le Bihan^{1,2}, Nathan Lack^{1,2}, Christopher Ong^{1,2}, Gang Wang⁴, Hao Zeng^{5*}, Colin Collins^{1,2*}, Yuzhuo Wang^{1,2,3*}

¹ Vancouver Prostate Centre, Vancouver, BC, Canada

² Department of Urologic Sciences, University of British Columbia, Vancouver, BC, Canada

³ Department of Basic and Translational Research, BC Cancer, Vancouver, BC, Canada

⁴ Department of Pathology and Laboratory Medicine, University of British Columbia, Vancouver, BC, Canada

⁵ Department of Urology, Institute of Urology, West China Hospital, Sichuan, University, Chengdu, China

⁶ These authors contribute equally

*Corresponding authors: Hao Zeng, kucaizeng@163.com; Colin Collins, colin.collins@ubc.ca; Yuzhuo Wang, ywang@bccrc.ca

Highlights:

1. Longitudinal single-cell RNA sequencing of treatment-induced adeno-to-NE transdifferentiation model revealed an intermediate transitional cell state in NEPC development and progression.
2. The sequential emergence of *ASCL1*^{high}/*FOXA2*^{low} and *ASCL1*^{low}/*FOXA2*^{high} NEPC subclusters indicates a temporal evolution of NEPC and highlights their role in contributing to NEPC heterogeneity.
3. *RUNX1T1*, a transcriptional regulator showing increased expression in both intermediate cell state and NEPCs, is identified as an early driver of NEPC development.
4. *RUNX1T1* plays important functional roles in promoting adeno-to-NE transdifferentiation in early phase of NEPC development and maintaining NE phenotype and aggressiveness in terminal NEPC.
5. Targeting *RUNX1T1* or its complex could offer new therapeutic strategies for NEPC management.

Abstract

Treatment-induced neuroendocrine prostate cancer (t-NEPC) is a lethal, castration-resistant subtype of prostate cancer. While t-NEPC typically arises from adenocarcinoma through neuroendocrine transdifferentiation after androgen pathway inhibition, the temporal dynamics and molecular drivers of this process remain poorly understood. Here, utilizing the first-in-field patient-derived xenograft (PDX) model of adenocarcinoma-to-NEPC transdifferentiation (LTL331/331R), we performed longitudinal single-cell transcriptomic sequencing (scRNA-seq) across seven timepoints spanning pre-castration to relapsed NEPC. Our analysis demonstrated 15 distinct cell clusters, including twelve adenocarcinoma clusters and two NEPC clusters (*ASCL1*^{high}/*FOXA2*^{low} and *ASCL1*^{low}/*FOXA2*^{high} clusters). Notably, we revealed a newly-discovered, early intermediate transitional cell state during t-NEPC development distinguished by epithelial-mesenchymal transition (EMT), stem cell-related, metabolically active, and HDAC-associated regulatory signatures. Analysis of this intermediate transitional cluster led to the identification of *RUNX1T1* as a pivotal transcriptional regulator of NEPC transdifferentiation. Functionally, *RUNX1T1* overexpression promoted AR pathway inhibition (ARPI) -induced NE transdifferentiation and increased resistance to ARPI treatment in prostate adenocarcinoma. *RUNX1T1* knockdown reverses the NE transdifferentiation, inhibits NEPC cell proliferation and induces apoptosis, and cell cycle arrest. In summary, this study identifies a critical intermediate transitional cell state during t-NEPC development and reveals the heterogeneity of terminal NEPC, offering new insights into NEPC biology and emphasizing the importance of early intervention. Moreover, the discovery of *RUNX1T1* as a key early driver active in both the initial and terminal phases of NEPC progression presents promising opportunities for therapeutic intervention.

Key Words: neuroendocrine prostate cancer; neuroendocrine transdifferentiation; transcriptional regulator; *RUNX1T1*; heterogeneity

Introduction:

Treatment-induced neuroendocrine prostate cancer (t-NEPC) is a highly aggressive and lethal subtype of advanced prostate cancer (PCa)^[1, 2]. It is characterized by a dynamic change in cell lineage phenotype, including a loss of androgen receptor (AR) and a gain of neuroendocrine (NE) markers, such as neural cell adhesion molecule 1 (NCAM1, CD56), chromogranin A (CHGA), and synaptophysin (SYP). It is thus resistant to AR pathway inhibition (ARPI)^[3-6].

Accumulating evidence indicates that the vast majority of clinical NEPCs are derived from prostatic adenocarcinoma following ADT via “NE transdifferentiation”, driven at least in part by AR-axis interference^[4, 7-9]. Recent advances in developing more potent ARPI (e.g., Enzalutamide, Abiraterone, and Apalutamide) have led to a dramatic rise in the clinical incidence of NEPC. Therefore, new therapeutic targets and more effective treatments are urgently needed to improve its clinical management^[10].

The research focusing on fully developed terminal NEPC has improved our understanding of NEPC and identified a few key molecules involved in NE phenotype and NEPC aggressiveness, which led to potential targeting therapeutic approaches under pre-clinical development currently. Although this approach is clearly important, the temporal development of NEPC, especially the contribution of early critical mediators that drive the development of NEPC is still unknown. We hypothesized that discovering and targeting early critical genes that drive the development of NEPC may be a more effective strategy, especially if such changes occur when a patient’s PCa can still be well-managed.

Given this, we developed the only available patient-derived xenograft (PDX) model of treatment-induced adenocarcinoma-to-NEPC transdifferentiation (LTL331/331R), which recapitulates the donor patient's disease progression in the clinic and provide a unique clinically relevant model for longitudinal study of t-NEPC development^[11-13]. In our previous study, integrated genomic and bulk transcriptomic analysis of this model demonstrated that NEPC arose through an adaptive transdifferentiation process in which transcriptional regulation plays an important role. Using this model, we and our collaborators have successfully identified/studied several critical genes involved in

NEPC development and progression (e.g., *HP1a*, *ONECUT2*, *BRN2*, *PEG10*, *SRRM4*, and PRC2 complex)^[11, 14-19].

In this study, to dissect the temporal heterogeneous cell state shift during NEPC development and identify key early drivers of NEPC, we performed longitudinal single-cell transcriptomic sequencing covering the entire process of adenocarcinoma-to-NEPC transdifferentiation. We successfully demonstrated the existence of an intermediate, transitional cell state in the early phase of NE transdifferentiation before the relapsed NEPC fully developed. Further investigation of this intermediate cell state led to the identification of *RUNX1T1* as a new important transcription regulator driving t-NEPC development^[20].

Results:

1. Single-cell RNA sequencing of the LTL331 PDX model demonstrates heterogeneous cell states during t-NEPC transdifferentiation

To unravel the evolutionary mechanism underlying treatment-induced neuroendocrine (NE) transdifferentiation, we exploited the single-cell transcriptomic profiling of LTL331/331R PDX model, which is the first-in-field and the only PDX model that recapitulates the entire NE transdifferentiation process from AR-positive prostatic adenocarcinoma (Adeno, LTL331) to AR-negative neuroendocrine prostate cancer (NEPC, LTL331R) after host castration, making this model a uniquely valuable model for studying t-NEPC^[11].

To systematically characterize the evolving landscape of tumor states during NE transdifferentiation at a single-cellular level, we collected tissues at seven time points (pre-castration; post-castration week 2, week 4, week 8, week 12, week 16 and relapsed) from LTL331/331R for single-cell transcription sequencing analysis.

Following rigorous quality control, we successfully collected 30,351 high-quality single-cell transcriptomes from cancer cells across seven LTL331/331R time-course samples. Unbiased clustering analysis identified fifteen discrete cell clusters, each of which exhibiting unique expression patterns, including twelve Adeno clusters (one AR^+/PSA^{high} ; eleven AR^+/PSA^{low} clusters), one $AR^{low}/PSA^-/NE^{low}$ cluster (cluster 14), and two NEPC clusters ($AR^-/PSA^-/NE^+$, cluster 10 and 13, Figure 1A-C). Notably, all NEPC clusters expressed luminal lineage keratin markers (*KRT8* and *KRT18*; Figure S1), strongly supporting the development of NEPC from Adeno via lineage reprogramming.

Subsequently, we computed AR activity and NE scores for all tumor clusters and ranked them accordingly (Figure 1D). As expected, in line with individual cell lineage markers expression patterns, Adeno clusters exhibited higher AR activity scores, with the pre-castration cluster 12 showing the highest. In contrast, NEPC clusters displayed lowest AR activity scores alongside markedly elevated NE scores. Cluster 14, a putative intermediate state, demonstrated both a loss of Adeno lineage (low AR activity) and a moderate gain of NE lineage, coupled with strong epithelial-mesenchymal transition (EMT, Figure 1D). These findings indicated a two-step neuroendocrine

transdifferentiation process. In the first phase, Adeno cells undergo dedifferentiation by suppressing AR-driven Adeno lineage programs and acquiring a multipotent, EMT-high state (cluster 14). In the second phase, they re-differentiate by activating NE-specific gene networks as they progress toward the terminal NEPC clusters (10 and 13). Thus, this intermediate cluster 14 might serve as a critical cell state bridging Adeno and NEPC. (Figure 1D-E).

2. Heterogeneous NEPC clusters represent cellular diversity in clinical NEPC patients

While NEPC is recognized as a distinct and aggressive subtype, the molecular drivers of its progression and intratumoral heterogeneity remain poorly understood. Through the comprehensive analysis of this sequencing, we identified two major subclusters in terminal relapsed NEPC tumors (Figure 2A-B). Cluster 10 was characterized by high expression of *ASCL1*, a known NE-related transcription factor, while the cluster 13 exhibited a low *ASCL1* but significantly high *FOXA2* expression. Temporal analysis revealed that these two subclusters emerged sequentially during the NEPC progression. *ASCL1*^{high} cells in cluster 10 appeared early in the castration-resistant phase (post-castration week 4) and persisted throughout neuroendocrine transdifferentiation, while *FOXA2*^{high} cells emerged later and dominated the terminal cluster 13 (Figure 3B). This pattern suggests a potential lineage relationship, where *ASCL1*^{high} cells may evolve into the terminal *FOXA2*^{high} population.

To validate the presence of similar NEPC heterogeneity in clinical samples, we analyzed publicly available single cell sequencing data from clinical NEPC patients [21]. Based on pathological characteristics, we re-analyzed three clinical NEPC samples and generated new UMAP plots (Figure 2C). We then calculated the NE score and *AR* expression for all cells, setting thresholds of negative *AR* expression and NE score > 0 to focus specifically on typical NEPC cancer cells for further analysis. Consistent with our findings in the LTL331/331R PDX model, we observed markedly higher *FOXA2* expression in *ASCL1*^{low} NEPC cells (Figure 2D). Furthermore, we confirmed the expression patterns of *ASCL1* and *FOXA2* in bulk RNA sequencing (RNA-seq) data

from clinical NEPC samples. By retrieving data from *AR*⁻/*NE*⁺ NEPC cases across various clinical cohorts, we demonstrated a negative correlation between *ASCL1* and *FOXA2* expression (Figure 2E). Additionally, we performed GSEA analysis of differentially expressed genes between cluster 10 and 13 and identified significantly enriched pathways/gene signatures in *ASCL1*^{high} and *FOXA2*^{high} clusters, respectively. Notably, the *FOXA2*^{high} cluster showed a marked enrichment of ribosome biogenesis pathways compared to the *ASCL1*^{high} cluster, indicative of an elevated protein synthesis state. This observation suggests that the *FOXA2*^{high} cluster represents a more advanced and aggressive stage of NEPC. Collectively, these findings support that the molecular heterogeneity captured in our PDX model mirrors the cellular diversity observed in clinical NEPC, thereby validating its translational significance.

3. Longitudinal analysis revealed a pivotal intermediate cell state during NE transdifferentiation

To delineate the dynamic transition from adenocarcinoma to NEPC, we performed longitudinal analysis of scRNA-seq data. First, we examined the distribution of the seven samples across all fifteen clusters at different time points (Figure 3A-B). Consistent with IHC data reported before, NE-like cells were absent in the pre-castration sample but emerged predominantly in late castration and relapsed NEPC tumors. Notably, the intermediate cluster 14 was absent in the pre-castration sample but appeared in both early and late post-castration samples, preceding the fully relapsed NEPC (Figure 3B; Table S1). To investigate the cell lineage relationships among cell clusters, we performed unbiased trajectory analysis using Monocle 3, which demonstrated that cluster 14 represents a critical transition point between Adeno and NEPC clusters (Figure 3C). Importantly, the expression of mixed cell lineage signatures, along with its timing of emergence during NE transdifferentiation and its transitional position in the trajectory analysis, strongly suggests that cluster 14 serves as a pivotal intermediate state, ultimately leading to the development of relapsed NEPC.

To gain deeper insights into this newly identified intermediate cluster, we further performed pathway enrichment analysis for relevant pathways (Figure 3D-F). Adeno,

NEPC, and cluster 14 exhibit distinct enrichment profiles for relevant pathways and demonstrate a gradual shift in the transition process. Notably, compared to fully relapsed NEPC clusters, cluster 14 showed reduced enrichment of neurodevelopmental/ glioma-associated pathways but upregulation of EMT, TGF- β -driven EMT, glioma mesenchymal, and stem cell-associated signatures (Figure 3D). Cluster 14 also displayed significant activation of multiple metabolic pathways, including bile acid metabolism, fatty acid metabolism, cholesterol homeostasis, glycolysis, and xenobiotic metabolism. This suggested that metabolic rewiring might support its intermediate transitional cellular state (Figure 3D). Additionally, enrichment of histone deacetylase (HDAC) regulatory pathways in cluster 14 underscores the importance of epigenetic remodeling in enabling lineage plasticity (Figure 3D). Comparing to Adeno clusters, cluster 14 demonstrated early activation of neuronal development and synapse formation signatures, alongside downregulation of prostate adenocarcinoma-associated signatures (Figure 3E-F). Notably, cluster 14 was also significantly enriched for EMT, cluster 14 also TGF- β -driven EMT, glioma mesenchymal, and stem cell-associated signatures, further underscoring its acquisition of mesenchymal and stem-like features as it transitions from adenocarcinoma toward NEPC. Collectively, these data reinforce cluster 14 as a metabolically active, epigenetically remodeled intermediate state marked by enhanced lineage plasticity along the adenocarcinoma-to-NEPC trajectory.

4. Identification of RUNX1T1 as a novel key driver of early treatment-induced neuroendocrine transdifferentiation

Since NEPC development is driven by an adaptive transdifferentiation process likely regulated by cell lineage-guiding transcription regulators, we hypothesized that the key transcription regulators responsible for cell identity shift are activated in both the early phase of NE transdifferentiation and terminal NEPC. To pinpoint these regulators, we analyzed 2,215 transcription regulators in the LTL331/331R model through comprehensive differential gene expression analyses^[22, 23].

Initially, we compared NEPC clusters and Adeno clusters and identified 55 transcription regulators with significantly differential expression (fold change>2, $p<0.001$), including well-studied NEPC-associated transcription factors (TFs) such as *SOX2*, *FOXA2*, *NKX2.2*, *INSM1*, and *ASCL1* (Figure 4A-B)^[19, 24-27]. Next, to investigate the changes in transcription regulators during the early stage of NE transdifferentiation, we compared cluster 14 with Adeno clusters and identified 30 significantly differentially expressed transcription regulators (Figure 4C). Among these genes, 14 transcription regulators showed the consistent expression trends in both the early phase of NE transdifferentiation and terminal NEPC, including 6 upregulated and 8 downregulated genes (Figure 4A). As expected, the downregulated ones included key Adeno lineage-related TFs such as *AR*, *FOXA1*, *GATA2*, and *NKX3-1*, consistent with the dedifferentiation process following AR pathway inhibition. Notably, the altered expression of those reported NE-related transcription regulators (i.e., *SOX2*, *FOXA2*, *NKX2.2*, *INSM1* and *ASCL1*) were only observed in the terminal NEPC clusters (cluster 10 and 13), but not during the early phase of NE transdifferentiation. Therefore, to pinpoint pivotal regulators driving early NE transdifferentiation and maintaining the NE phenotype in terminal NEPC, we focused on the genes showing increased expression in both cluster 14 as an early event during NEPC development and terminal NEPC clusters 10 and 13. Among these genes, *RUNX1T1*, a transcriptional regulator previously unreported in NEPC, emerged as the top-ranked candidate for the following study.

We first confirmed the expression of *RUNX1T1* in the LTL331/331R PDX model, where it was significantly upregulated in cluster 10, 13 and 14 (Figure 4D). We then validated that *RUNX1T1* expression is markedly increased in multiple independent NEPC cell lines and PDXs compared to non-NEPC ones (Figure 4E-G). Furthermore, across three independent clinical cohorts, *RUNX1T1* is consistently upregulated in NEPC patients and strongly correlated with NE lineage markers expression, as evidenced by bulk sequencing data (Figure 4H).

5. RUNX1T1 promotes ARPI-induced NE transdifferentiation in prostate adenocarcinoma

To assess the functional role of RUNX1T1 in driving early NE transdifferentiation, we investigated whether its overexpression in Adeno cells could induce the NE phenotype under ARPI treatment. We first ectopically overexpressed RUNX1T1 (RUNX1T1-OE) in V16D cells, a CRPC adenocarcinoma cell line derived from LNCaP (Figure 5A). We then examined the expression of cell surface NE marker, NCAM1, via flow cytometry in control and RUNX1T1-OE V16D cells after 2 weeks of culture with FBS and Enzalutamide (Enza), respectively. Under normal condition, a slight increase in NCAM1 expression was observed between the control and OE groups (mean fluorescence intensity, MFI: control, 134; RUNX1T1, 146 and 200). After 2 weeks of Enza treatment, RUNX1T1-OE cells showed a dramatic upregulation of NCAM1 compared to the control (MFI: control, 327; RUNX1T1, 551 and 517; Figure 5B-C). Furthermore, we validated the consistent results obtained from flow cytometry through qPCR and immunoblotting (Figure 5D-E). Collectively, these findings highlight its ability to promote Adeno cells to acquire the NE phenotype under long-term Enza treatment.

In addition, as the cell lineage plasticity (i.e., NE transdifferentiation) is considered a resistance mechanism towards ADT/ARPI in PCa, we proceeded to determine whether RUNX1T1 confers resistance to the Enza treatment. To investigate the impact of RUNX1T1 on the sensitivity of Adeno cell to Enza treatment, we assessed the cell viability of control and RUNX1T1-OE V16D cells under two different culture conditions (FBS or Enza, Figure 5F; S5). While RUNX1T1 overexpression did not enhance cell viability under FBS conditions, it significantly improve cell survival and increased resistance to Enza treatment compared to controls.

6. RUNX1T1 knockdown reverses the NE transdifferentiation, inhibits NEPC cell proliferation, induces apoptosis, and cell cycle arrest.

Given the marked upregulation of RUNX1T1 in both early NEPC development and terminal NEPC, we further explored its role in maintaining the NE phenotype and cell survival ability in terminal NEPC, evaluating its potential as a target for this aggressive PCa subtype. We constructed stable inducible RUNX1T1 knockdown cell line in H660

cells using lentiviral vectors (H660-ShRUNX1T1-1 and H660-ShRUNX1T1-2; Figure 6A-B). Compared to the H660 control cells H660-ShNC, RUNX1T1 knockdown in H660 cells significantly diminished the NE phenotype by reducing the expression of NCAM1, NSE and ASCL1 at both mRNA and protein levels. In addition, upon RUNX1T1 knockdown, the viability of H660 cells was significantly impaired, ultimately leading to significant cell death within three weeks of passaging (Figure 6C).

To further elucidate the effects of RUNX1T1 knockdown, we assessed its impact on the cell cycle and apoptosis of H660 cells using flow cytometry. The flow cytometry results using EdU-staining assay revealed a significant reduction in the number of EdU-positive cells in H660 cells following RUNX1T1 knockdown, indicating the critical role of RUNX1T1 in maintaining proliferation in H660 cells (Figure 6D). Furthermore, apoptosis assays demonstrated that knocking down RUNX1T1 promoted apoptosis in H660 cells, further impairing the survival ability of these cells (Figure 6E).

Additionally, we performed RNA-seq on H660-ShRUNX1T1 cells and conducted pathway enrichment analysis for common cancer-related pathways. Gene pathway enrichment analysis indicate that many pathways involved in neuron development were significantly downregulated in H660-ShRUNX1T1 cells (Figure 6F). Moreover, the NEPC-associated signature based on published studies were notably downregulated in these cells, highlighting the pivotal role of RUNX1T1 in maintaining the terminal NEPC phenotype (Figure 6H). Interestingly, hallmark enrichment analysis revealed that upregulated features in H660-ShRUNX1T1 cells highly resembled those of cluster 14 in the LTL331/331R, particularly within the EMT pathway (Figure 6G and 6I). By comparing cluster 14 with NEPC cell cluster, we identified the top 50 upregulated genes to establish the cluster 14 signature, which was significantly enriched in H660-ShRUNX1T1 cells compared to H660-ShNC cells (Figure 6J).

Discussion

Accumulating evidence suggests that treatment-induced NEPC arises by transdifferentiation of prostatic adenocarcinoma rather than clonal selection of cells originating from NE cells after hormonal therapy. However, limited clinically relevant models are available to mimic the treatment-induced NE transdifferentiation. It has been

reported that key genetic alterations can spontaneously induce NEPC development from prostate luminal cells in GEMMs (TKO models), albeit in the absence of ADT. In contrast, the LTL331 model maintained typical adenocarcinoma features in intact hosts (>20 generations) and consistently developed into NEPC only after host castration, which mimics the donor patient's t-NEPC progression in the clinic. In this study, the histopathological and single-cell transcriptome analysis confirms the absence of NE-like cells in pre-castration samples, gradual post-castration cell state shift, and multi-clonal development of NEPC in late post-castration time points and provides strong evidence supporting the NE transdifferentiation process from prostatic adenocarcinoma. Given this, the LTL331/331R model recapitulates the t-NEPC development process in the clinic and provides a valuable clinically relevant tool for studying t-NEPC.

The relapsed LTL331R tumor consistently exhibits full NEPC features, such as high expression of a panel of NE markers (NCAM1, CHGA, and SYP), a high NE signature score, and the absence of AR. Interestingly, single-cell RNA seq data reveal two different NE cell states, i.e. $ASCL1^{high}/FOXA2^{low}$ and $ASCL1^{low}/FOXA2^{high}$, in the relapsed LTL331R tissue, which displayed distinct transcriptomic profiles. The $ASCL1^{low}$ NEPC cells did not express the markers associated with $ASCL1^{low}$ SCLC subtypes (*NEUROD1* and *POU2F3*) nor the previously reported markers of $ASCL1^{low}$ NEPC subtypes (*ASCL2* and *NFIB*). Notably, *FOXA2* was highly expressed predominantly in $ASCL1^{low}$ cluster, but not in $ASCL1^{high}$ clusters. The sequential emergence of these two NEPC clusters suggesting that the $ASCL1^{high}$ NEPC cluster may evolve into the more terminal $FOXA2^{high}$ NEPC cluster indicating a temporal evolution of NEPC and highlights their role in contributing to NEPC heterogeneity. Consistent with our findings in PDX models, the existence of $ASCL1^{high}/FOXA2^{low}$ and $ASCL1^{low}/FOXA2^{high}$ NEPC states/phenotypes was confirmed in clinical NEPC samples.

Due to the limited availability of scRNA-seq data for clinical NEPC samples and the inherent heterogeneity of bulk RNA-seq data, we could not definitively confirm the prevalence of mutually exclusive subtypes defined by these two transcription regulators. Additionally, we were unable to validate the temporal changes in NEPC cell states in clinical samples because no time course studies of clinical NEPC have been conducted.

Additional single-cell sequencing data from clinical NEPC samples would be valuable for validating such NEPC subtypes. Further investigation into the ASCL1 and FOXA2 regulons in each NEPC subtype, along with their mutual regulation, will offer insights into NEPC development, leading to a better understanding of NEPC subtype-specific vulnerabilities and eventually pave the way for developing subtype-specific therapies.

NE transdifferentiation, a phenotype transformation from adenocarcinoma to neuroendocrine prostate cancer, is generally divided into two main processes. The early stage of NE transdifferentiation usually involves de-differentiation, enabling the tumor to shed the original AR-driven lineage and acquire highly plastic, stem-like features. The later stage involves re-differentiation, resulting in the acquisition of NE-like pathological phenotype. Current research in NEPC primarily focuses on elucidating and targeting mechanisms of resistance during the terminal stage of the disease, leading to the identification of several key molecular players involved at this late phase. However, we propose that uncovering and targeting critical genes driving early NE transdifferentiation could not only enhance our understanding of NEPC pathogenesis but also provide novel therapeutic targets for early intervention. This approach is particularly compelling, as patients with prostate cancer may still be in a clinically manageable state during the initial stages of NE transdifferentiation, offering a window of opportunity for more effective treatment. To explore the early change of NEPC development, we performed longitudinal single-cell RNA seq analysis of the LTL331/331R model. As expected, we observed a progressive cell state shift in the early phase of host castration, representing a common de-differentiation response of adenocarcinoma cells (characterized by a continuous loss of luminal/AR activity signature). Importantly, we observed a highly plastic transitional cell state during NEPC development. This unique transitional intermediate cluster in the LTL331 model showed the expression of mixed cell lineage signatures and strong EMT features. It is consistent with the extraordinarily high lineage plasticity of LTL331 compared to other adenocarcinoma PDX models, which developed into AR⁺ CRPC after host castration. In addition, this intermediate cluster also demonstrated higher NE-related signature compared to adenocarcinoma clusters. These data, along with the timing of its emergence during the LTL331/331R time course and its transitional position in trajectory analysis, strongly support its pivotal transitional

state during NEPC development and provide new biological insights into the development of t-NEPC. This marks the first identification of an intermediate stage at the single-cell resolution during NE transdifferentiation, offering novel biological insights into the progression of t-NEPC. Our study further characterizes this transitional phase, highlighting its potential utility as a prognostic marker for stratifying adenocarcinoma patients and predicting their susceptibility to t-NEPC transformation. Importantly, by leveraging this newly defined transitional state, we identified *RUNX1T1* as a novel early driver of t-NEPC.

RUNX1T1 is a member of the MTG family, which plays a crucial role in neurogenesis. In cancer field, initially, *RUNX1T1* was identified as a partner gene of *AML1* (also called *RUNX1*) to form the fusion gene *AML1-ETO* (*RUNX1-RUNX1T1*) in acute myeloid leukemia (AML) and is considered a leukemia-initiating driver event^[25, 28]. In this fusion gene, *RUNX1T1* (*ETO*) serves as an inhibitory platform for different HDAC family members to form repressive complex and suppresses *AML1*-regulating downstream genes via deacetylation, thus promoting carcinogenesis^[29, 30]. However, the role of *RUNX1T1* alone in other types of cancer is very limited. In bladder cancer, *RUNX1T1* could form the repressive complex with *TCF4*, suppress the transcription of *miR-625-5p* and therefore promote bladder cancer progression^[31]. Recently, it's reported that silencing *RUNX1T1* inhibits cell viability and tumor growth in neuroblastoma and small cell lung cancer cells^[32, 33]. However, its function and role in PCa is unknown.

To our knowledge, this is the first study of *RUNX1T1* in prostate cancer. We observed that *RUNX1T1* is absent in prostatic adenocarcinoma but is widely and highly expressed in NEPC. Specifically, in our longitudinal study using the LTL331/331R model, we found that *RUNX1T1* is highly expressed in the early transitional stage (intermediate cluster 14) and the terminal NEPC (clusters 10 and 13), contrasting with its absence in any adenocarcinoma clusters. Interestingly, the intermediate NEPC cell state and increased expression of *RUNX1T1* are not observed in other PDXs that develop into AR+CRPC after host castration, which supports the specific role of *RUNX1T1* in NE transdifferentiation. *RUNX1T1* can form complexes with other TFs and bind to genomic DNA, globally regulating the epigenetic landscape through recruiting

the HDAC family. As a known epigenetic regulator, RUNX1T1 has the ability to act as an upstream core factor in the complicated and multi-step process of NE transdifferentiation, which involves coordinated alternation of multiple genes.

Considering these, we propose that *RUNX1T1* could serve as a potential biomarker of early NEPC transdifferentiation for predicting the response of ADT for PCa patients and their susceptibility to NEPC development. Our study provides preliminary evidence that upregulation of RUNX1T1 in prostatic adenocarcinoma cells is associated with an enhanced neuroendocrine phenotype and an increased propensity for resistance to ARPI. These functional findings support the role of RUNX1T1 as an early driver of NEPC development. Future studies incorporating clinical cohorts with longitudinal sampling from patients who develop t-NEPC will be critical for further validating RUNX1T1 as a potential early biomarker for t-NEPC development and for improving patient stratification strategies.

In summary, our study presents a high-resolution single-cell transcriptional atlas and provides the first longitudinal characterization of NE transdifferentiation in a clinically relevant t-NEPC model. Using longitudinal scRNA-seq, we identified a previously unrecognized intermediate transitional cell state that emerges during the progression from prostate adenocarcinoma to NEPC. This transitional population marks a critical step in NEPC development and provides novel insight into the dynamic nature of lineage plasticity. Further observation of the sequential emergence of two distinct NEPC subcluster, *ASCL1^{high}/FOXA2^{low}* and *ASCL1^{low}/FOXA2^{high}*, suggests a temporal evolution of NEPC and highlights their contributions to tumor heterogeneity. These findings offer a refined view of NEPC progression and reveal cellular diversity that may underlie differential therapeutic vulnerabilities. Through integrative analysis, we identified *RUNX1T1* as a transcriptional regulator upregulated in both the transitional cell state and established NEPC. Functional studies support its role as an early driver of NEPC, promoting adeno-to-NE transdifferentiation in the initial phase of lineage switching and sustaining NE phenotype and aggressiveness in terminal-stage NEPC. Collectively, our findings establish RUNX1T1 as a central player in NEPC pathogenesis. Targeting RUNX1T1 or its associated corepressor complexes represents a promising

therapeutic strategy for intercepting NEPC development and improving clinical management of this aggressive disease subtype.

Acknowledgments

This research was supported in part by the Canadian Institutes of Health Research (#153081, #173338, #180554, #186331), Terry Fox Research Institute (#1109), US Department of Defense (DoD #W81XWH-21-1-0300), A PNW Prostate Cancer SPORE (P50 CA097186) pilot grant, a Canadian Cancer Society Breakthrough Team Grant generously supported by the Lotte & John Hecht Memorial Foundation (CCS grant #707683), the BC Cancer Foundation (grant #1PRRG012), and a financial support from the program of China Scholarships Council (to YN, NO. 202206240124).

Author contributions

Y.C. Ni, D. Lin, M.C. Shi, Y.Y. Lin, H. Zeng, C. Collins, and Y.Z. Wang conceptualized and designed the study. Y.C. Ni, D. Lin, M.C. Shi, and Y.Y. Lin developed the methodology and performed the experiments. Y.C. Ni, D. Lin, M.C. Shi, Y.Y. Lin, H. Xue, X. Dong, L.L. Liu, F. Sar, R. Wu, T. Morova, A. Haegert, R. Bell, A. Classen, X.Y. Pang, Y. Wang, J.R. Chen, S. Volik, S.L. B., N. Lack, G. Wang and C. Ong were responsible for data acquisition, including provision of animals, and management, and facility support. Data analysis and interpretation were carried out by Y.C. Ni, D. Lin, M.C. Shi, Y.Y. Lin, X.Y. Pang, and A. Classen. The manuscript was drafted and revised by Y.C. Ni, D. Lin, M.C. Shi, Y.Y. Lin, H. Zeng, C. Collins, and Y.Z. Wang. H. Zeng, C. Collins, and Y.Z. Wang supervised the project.

Methods

PDXs and clinical datasets

LTL331 PDXs were established as previously described^[12]. After host castration, tissue was harvested, measured, fixed for histopathology, and processed for single-cell RNA analysis.

Single-cell RNA sequencing

Tumor specimens were first finely minced with a Bard-Parker scalpel and then enzymatically dissociated into a single-cell suspension using the Miltenyi Biotec human tumor dissociation kit, following the manufacturer's protocol. The dissociation cell suspension was washed and resuspended in phosphate-buffered saline (1× PBS; Gibco) containing 0.04% BSA (Miltenyi Biotec). Cell counts and viability assessments were performed by staining with 0.4% Trypan Blue (Thermo Fisher), and only samples exhibiting at least 80% viable cells were advanced to single-cell RNA sequencing. Approximately 10,000 cells per sample were loaded onto the 10× Genomics Chromium Controller, and the single cell libraries were constructed using the Chromium Single Cell 3' v3.1 chemistry according to the supplier's protocol. Sequencing was carried out on the Complete Genomics DNB-Seq G400 platform, targeting an average depth of 47,760 reads per cell.

Cell culture and treatment

239T, LNCaP, PC3, DU145, 22Rv1 and NCI-H660 cells were obtained from the American Type Culture Collection (ATCC). Cells were authenticated with the fingerprinting method at Fred Hutchinson Cancer Research Centre. V16D cells were provided by courtesy of Dr. Amina Zoubeydi. Mycoplasma testing was routinely performed at the Vancouver Prostate Centre (VPC). NCI-H660 cells were cultured in RPMI-1640 medium (Gibco) with supplements as follows: 5% FBS (Gibco), 10 nmol/L b-estradiol (Sigma), 10 nmol/L Hydrocortisone (Sigma), and 1% Insulin-Transferrin-Selenium (Thermo Fisher). LNCaP, PC3, DU145, 22Rv1 and V16D cells were maintained in RPMI-1640 containing 10% FBS. 293T cells were kept in DMEM (Gibco) with 10% FBS. For in vitro NE phenotype induction in V16D cells, cells were starved with phenol-red-free RPMI-1640 (Gibco) containing 10% charcoal-stripped serum

(CSS; Gibco) for 24 hours, and then cultured in the same medium with the addition of 10 mmol/L Enzalutamide (Medchem Express, cat# HY-70002) for another 2 weeks.

Immunohistochemistry (IHC) Staining

Formalin-fixed, paraffin-embedded tissue sections were cut at 5 µm thickness, deparaffinized in xylene, and rehydrated through a graded ethanol series. Antigen retrieval was performed by heating slides in 10 mM citrate buffer (pH 6.0) using a pressure cooker for 10 minutes. After cooling to room temperature, endogenous peroxidase activity was blocked with 3% hydrogen peroxide for 10 minutes. Sections were then incubated with 5% normal goat serum for 30 minutes to reduce nonspecific binding.

Primary antibodies were applied and incubated overnight at 4°C. The following antibodies were used: anti-RUNX1T1(Proteintech, cat#15494-1-AP), anti-NCAM1/CD56 (Cell Marque, cat##156R).

Western blotting

Western blotting was performed by resolving protein lysates on SDS-PAGE gels, transferring them onto PVDF membranes, and blocking with Tris-buffered saline/Tween 20 (TBST) containing 5% skim milk for 1 hour at room temperature.

The following primary antibodies were used: anti-RUNX1T1(Proteintech, cat#15494-1-AP), anti-anti-NCAM1/CD56 (Cell Signaling Technology, cat#3576), anti-CHGA (Cell Signaling Technology, cat# 60893), anti-SYP (Santa Cruz Biotechnology, cat#sc-17750), anti-ASCL1 (Santa Cruz Biotechnology, cat# sc-374104), anti-Actin (Sigma-Aldrich, cat# A5441), anti-SOX2 (Cell Signaling Technology, cat#3579), anti-Vinculin (Sigma-Aldrich, cat#V9131).

Plasmid Transfection and Lentiviral transfection.

For overexpression studies, plasmids were transfected using Lipofectamine™ 3000 reagent (Thermo Fisher Scientific, cat# L3000008) following the manufacturer's instructions. The RUNX1T1 overexpression plasmid (TFORF1679, Addgene#143835) and the corresponding GFP vector control (TFORF3549, Addgene#145025) were used in these experiments.

To knock down RUNX1T1 expression in NCI-H660 cell line, two short hairpin RNA (shRNA) constructs were designed to target the following sequences: shRNA#1 (CACCGAATGACATTTACCCGAGAT) and shRNA#2 (CACCGCTGTGCAATACCTTCAAAAA). These sequences were cloned into the doxycycline-inducible tet-pLKO-puro plasmid (Addgene #21915), generating tet-pLKO-RUNX1T1-shRNA#1 and tet-pLKO-RUNX1T1-shRNA#2 constructs. Stable cell lines were established and treated with 1 µg/mL doxycycline to induce shRNA expression for subsequent validation and functional assays.

RNA Preparation and RT-qPCR

Total RNA was extracted from cells or organoids following the indicated treatments using the RNeasy Plus Mini Kit (Qiagen, cat# 74034) according to the manufacturer's instructions. One microgram of RNA was reverse transcribed into cDNA using QuantiTect Reverse Transcription Kit (Qiagen, cat#205313). Quantitative real-time PCR (RT-qPCR) was performed using the Applied Biosystems™ QuantStudio™ 7 Pro. Data were analyzed using Design and Analysis Software version 2.8.0 (Life Technologies).

RNA sequencing (RNA-Seq) and Pathway Analysis

Total RNA was extracted from NCI-H660 cells stably expressing shNC or shRUNX1T1 following treatment with 1 µg/mL doxycycline for 8 days, using the RNeasy Plus Mini Kit (Qiagen) as described above. RNA libraries were prepared and sequenced by

Novogene on the Illumina NovaSeq 6000 platform, generating 150 bp paired-end reads with a depth of 20 million reads per sample.

Sequencing reads were aligned to the GRCh38 reference genome using HISAT2 (version 2.0.5). Gene expression was quantified using featureCounts (v1.5.0-p3), and expression levels were normalized to Fragments Per Kilobase of transcript per Million mapped reads (FPKM) to account for variations in gene length and sequencing depth. Differential gene expression analysis was performed using the DESeq2 package (version 1.20.0) in R. Genes with an adjusted *P*-value ≤ 0.05 were considered differentially expressed. The RNA-seq dataset for *RUNX1T1* knockdown data reported in this article is deposited in NCBI GEO (GSE*****).

Pathway analysis was carried out using Gene Set Enrichment Analysis (GSEA) (version 4.3.2), applying the weighted enrichment statistic to normalized gene counts. Genes were ranked based on \log_2 fold change for enrichment scoring.

Cell Viability Assay

Cell viability at various time points was assessed using the Cell Counting Kit-8 (CCK-8; Dojindo Laboratories, cat# CK04) following the manufacturer's instructions. Briefly, cells were seeded in 96-well plates with doxycycline and incubated overnight. On the designated day, 20 μ L of CCK-8 reagent was added to each well containing 200 μ L of culture medium (1:10 ratio). Plates were incubated for 3 hours at 37°C in a humidified incubator with 5% CO₂. Following incubation, absorbance at 450 nm was measured to determine cell viability, reflecting metabolic activity and, by extension, the number of viable cells.

Incucyte Live-Cell Imaging

Real-time cell proliferation and confluence were monitored using the Incucyte® Live-Cell Analysis System (Sartorius). Cells were seeded into 96-well plates at an optimized density and allowed to adhere overnight. Plates were placed into the Incucyte system, maintained at 37°C in a humidified atmosphere with 5% CO₂, and imaged every 12 hours over the course of the experiment using the 10× objective. Phase-contrast images

were collected from multiple regions per well, and cell confluence was automatically quantified using the Incucyte integrated image analysis software.

Apoptosis Assay

Apoptosis was evaluated using BD Pharmingen™ FITC Annexin V Apoptosis Detection Kit I (#556547) according to the manufacturer's protocol. Briefly, cells were harvested after 7 days of doxycycline-induced knockdown and stained with 5 μ L Annexin V and 5 μ L propidium iodide (PI) for 15 minutes at room temperature. Samples were analyzed using an LSRFortessa II flow cytometer (BD Biosciences) to detect Annexin V and PI signals. Unstained controls and single-stained samples (Annexin V or PI) were used to define gating parameters for the identification of apoptotic populations.

EdU Assay

Cell proliferation was assessed by EdU incorporation using the EdU Staining Proliferation Kit (iFluor 488) (Abcam ab219801), following the manufacturer's instructions. Briefly, cells were pulsed with 10 μ M EdU for 3 hours at the indicated time points. After incubation, cells were fixed, permeabilized, and stained to label S-phase cells that had incorporated EdU. Flow cytometric analysis was performed using an LSRFortessa II (BD Biosciences) to quantify the percentage of EdU-positive cells. Cells not exposed to EdU were used as a negative control to define the gating strategy for EdU-positive populations.

REFERENCES:

1. Wang Y, Wang Y, Ci X, Choi SYC, Crea F, Lin D, Wang Y: **Molecular events in neuroendocrine prostate cancer development.** *Nat Rev Urol* 2021, **18**(10):581-596.
2. Beltran H, Rickman DS, Park K, Chae SS, Sboner A, MacDonald TY, Wang Y, Sheikh KL, Terry S, Tagawa ST *et al*: **Molecular characterization of neuroendocrine prostate cancer and identification of new drug targets.** *Cancer Discov* 2011, **1**(6):487-495.
3. Yamada Y, Beltran H: **Clinical and Biological Features of Neuroendocrine Prostate Cancer.** *Curr Oncol Rep* 2021, **23**(2):15.
4. Wang HT, Yao YH, Li BG, Tang Y, Chang JW, Zhang J: **Neuroendocrine Prostate Cancer (NEPC) progressing from conventional prostatic adenocarcinoma: factors associated with time to development of NEPC and survival from NEPC diagnosis-a systematic review and pooled analysis.** *J Clin Oncol* 2014, **32**(30):3383-3390.
5. Conteduca V, Oromendia C, Eng KW, Bareja R, Sigouros M, Molina A, Faltas BM, Sboner A, Mosquera JM, Elemento O *et al*: **Clinical features of neuroendocrine prostate cancer.** *Eur J Cancer* 2019, **121**:7-18.
6. Zhang Q, Han Y, Zhang Y, Liu D, Ming J, Huang B, Qiu X: **Treatment-Emergent Neuroendocrine Prostate Cancer: A Clinicopathological and Immunohistochemical Analysis of 94 Cases.** *Front Oncol* 2020, **10**:571308.
7. Beltran H, Prandi D, Mosquera JM, Benelli M, Puca L, Cyrta J, Marotz C, Giannopoulou E, Chakravarthi BV, Varambally S *et al*: **Divergent clonal evolution of castration-resistant neuroendocrine prostate cancer.** *Nat Med* 2016, **22**(3):298-305.
8. Davies AH, Beltran H, Zoubeidi A: **Cellular plasticity and the neuroendocrine phenotype in prostate cancer.** *Nat Rev Urol* 2018, **15**(5):271-286.
9. Maylin ZR, Smith C, Classen A, Asim M, Pandha H, Wang Y: **Therapeutic Exploitation of Neuroendocrine Transdifferentiation Drivers in Prostate Cancer.** *Cells* 2024, **13**(23).
10. Okasho K, Ogawa O, Akamatsu S: **Narrative review of challenges in the management of advanced neuroendocrine prostate cancer.** *Transl Androl Urol* 2021, **10**(10):3953-3962.
11. Akamatsu S, Wyatt AW, Lin D, Lysakowski S, Zhang F, Kim S, Tse C, Wang K, Mo F, Haegert A *et al*: **The Placental Gene PEG10 Promotes Progression of Neuroendocrine Prostate Cancer.** *Cell Rep* 2015, **12**(6):922-936.
12. Lin D, Wyatt AW, Xue H, Wang Y, Dong X, Haegert A, Wu R, Brahmbhatt S, Mo F, Jong L *et al*: **High fidelity patient-derived xenografts for accelerating prostate cancer discovery and drug development.** *Cancer Res* 2014, **74**(4):1272-1283.
13. Shi M, Wang Y, Lin D, Wang Y: **Patient-derived xenograft models of neuroendocrine prostate cancer.** *Cancer Lett* 2022, **525**:160-169.
14. Ci X, Hao J, Dong X, Choi SY, Xue H, Wu R, Qu S, Gout PW, Zhang F, Haegert AM *et al*: **Heterochromatin Protein 1 α Mediates Development and Aggressiveness of Neuroendocrine Prostate Cancer.** *Cancer Res* 2018, **78**(10):2691-2704.
15. Guo H, Ci X, Ahmed M, Hua JT, Soares F, Lin D, Puca L, Vosoughi A, Xue H, Li E *et al*: **ONECUT2 is a driver of neuroendocrine prostate cancer.** *Nat Commun* 2019, **10**(1):278.
16. Bishop JL, Thaper D, Vahid S, Davies A, Ketola K, Kuruma H, Jama R, Nip KM, Angeles A, Johnson F *et al*: **The Master Neural Transcription Factor BRN2 Is an Androgen Receptor-Suppressed Driver of Neuroendocrine Differentiation in Prostate Cancer.** *Cancer Discov* 2017, **7**(1):54-71.
17. Li Y, Donmez N, Sahinalp C, Xie N, Wang Y, Xue H, Mo F, Beltran H, Gleave M, Wang Y *et al*: **SRRM4 Drives Neuroendocrine Transdifferentiation of Prostate Adenocarcinoma Under Androgen Receptor Pathway Inhibition.** *Eur Urol* 2017, **71**(1):68-78.
18. Clermont PL, Lin D, Crea F, Wu R, Xue H, Wang Y, Thu KL, Lam WL, Collins CC, Wang Y *et al*: **Polycomb-mediated silencing in neuroendocrine prostate cancer.** *Clin Epigenetics* 2015, **7**(1):40.

19. Wang Y, Xue H, Zhu X, Lin D, Chen Z, Dong X, Chen J, Shi M, Ni Y, Cao J *et al*: **Deciphering the Transcription Factor Landscape in Prostate Cancer Progression: A Novel Approach to Understand NE Transdifferentiation.** *Adv Sci (Weinh)* 2025:e2404938.
20. Wang Y, Scurll J, Rascón IA, Cui C, Ni Y, Shi AM, Gangadharannambiar P, Wang Y, Akamatsu S, Beltran H *et al*: **The third symposium on treatment-induced neuroendocrine prostate cancer: insights and future directions.** *Epigenomics* 2024, **16**(17):1129-1132.
21. Dong B, Miao J, Wang Y, Luo W, Ji Z, Lai H, Zhang M, Cheng X, Wang J, Fang Y *et al*: **Single-cell analysis supports a luminal-neuroendocrine transdifferentiation in human prostate cancer.** *Commun Biol* 2020, **3**(1):778.
22. Krämer A, Green J, Pollard J, Jr., Tugendreich S: **Causal analysis approaches in Ingenuity Pathway Analysis.** *Bioinformatics* 2014, **30**(4):523-530.
23. Lambert SA, Jolma A, Campitelli LF, Das PK, Yin Y, Albu M, Chen X, Taipale J, Hughes TR, Weirauch MT: **The Human Transcription Factors.** *Cell* 2018, **175**(2):598-599.
24. Nouruzi S, Ganguli D, Tabrizian N, Kobelev M, Sivak O, Namekawa T, Thaper D, Baca SC, Freedman ML, Aguda A *et al*: **ASCL1 activates neuronal stem cell-like lineage programming through remodeling of the chromatin landscape in prostate cancer.** *Nat Commun* 2022, **13**(1):2282.
25. Romero R, Chu T, González Robles TJ, Smith P, Xie Y, Kaur H, Yoder S, Zhao H, Mao C, Kang W *et al*: **The neuroendocrine transition in prostate cancer is dynamic and dependent on ASCL1.** *Nat Cancer* 2024, **5**(11):1641-1659.
26. Han M, Li F, Zhang Y, Dai P, He J, Li Y, Zhu Y, Zheng J, Huang H, Bai F *et al*: **FOXA2 drives lineage plasticity and KIT pathway activation in neuroendocrine prostate cancer.** *Cancer Cell* 2022, **40**(11):1306-1323.e1308.
27. Mu P, Zhang Z, Benelli M, Karthaus WR, Hoover E, Chen CC, Wongvipat J, Ku SY, Gao D, Cao Z *et al*: **SOX2 promotes lineage plasticity and antiandrogen resistance in TP53- and RB1-deficient prostate cancer.** *Science* 2017, **355**(6320):84-88.
28. Davis JN, McGhee L, Meyers S: **The ETO (MTG8) gene family.** *Gene* 2003, **303**:1-10.
29. Martinez-Soria N, McKenzie L, Draper J, Ptasinska A, Issa H, Potluri S, Blair HJ, Pickin A, Isa A, Chin PS *et al*: **The Oncogenic Transcription Factor RUNX1/ETO Corrupts Cell Cycle Regulation to Drive Leukemic Transformation.** *Cancer Cell* 2019, **35**(4):705.
30. Hug BA, Lazar MA: **ETO interacting proteins.** *Oncogene* 2004, **23**(24):4270-4274.
31. Yin YW, Liu KL, Lu BS, Li W, Niu YL, Zhao CM, Yang Z, Guo PY, Qi JC: **RBM24 exacerbates bladder cancer progression by forming a Runx1t1/TCF4/miR-625-5p feedback loop.** *Exp Mol Med* 2021, **53**(5):933-946.
32. Murray JE, Valli E, Milazzo G, Mayoh C, Gifford AJ, Fletcher JI, Xue C, Jayatilleke N, Salehzadeh F, Gamble LD *et al*: **The transcriptional co-repressor Runx1t1 is essential for MYCN-driven neuroblastoma tumorigenesis.** *Nat Commun* 2024, **15**(1):5585.
33. He T, Wildey G, McColl K, Savadelis A, Spainhower K, McColl C, Kresak A, Tan AC, Yang M, Abbas A *et al*: **Identification of RUNX1T1 as a potential epigenetic modifier in small-cell lung cancer.** *Mol Oncol* 2021, **15**(1):195-209.

Figure 1

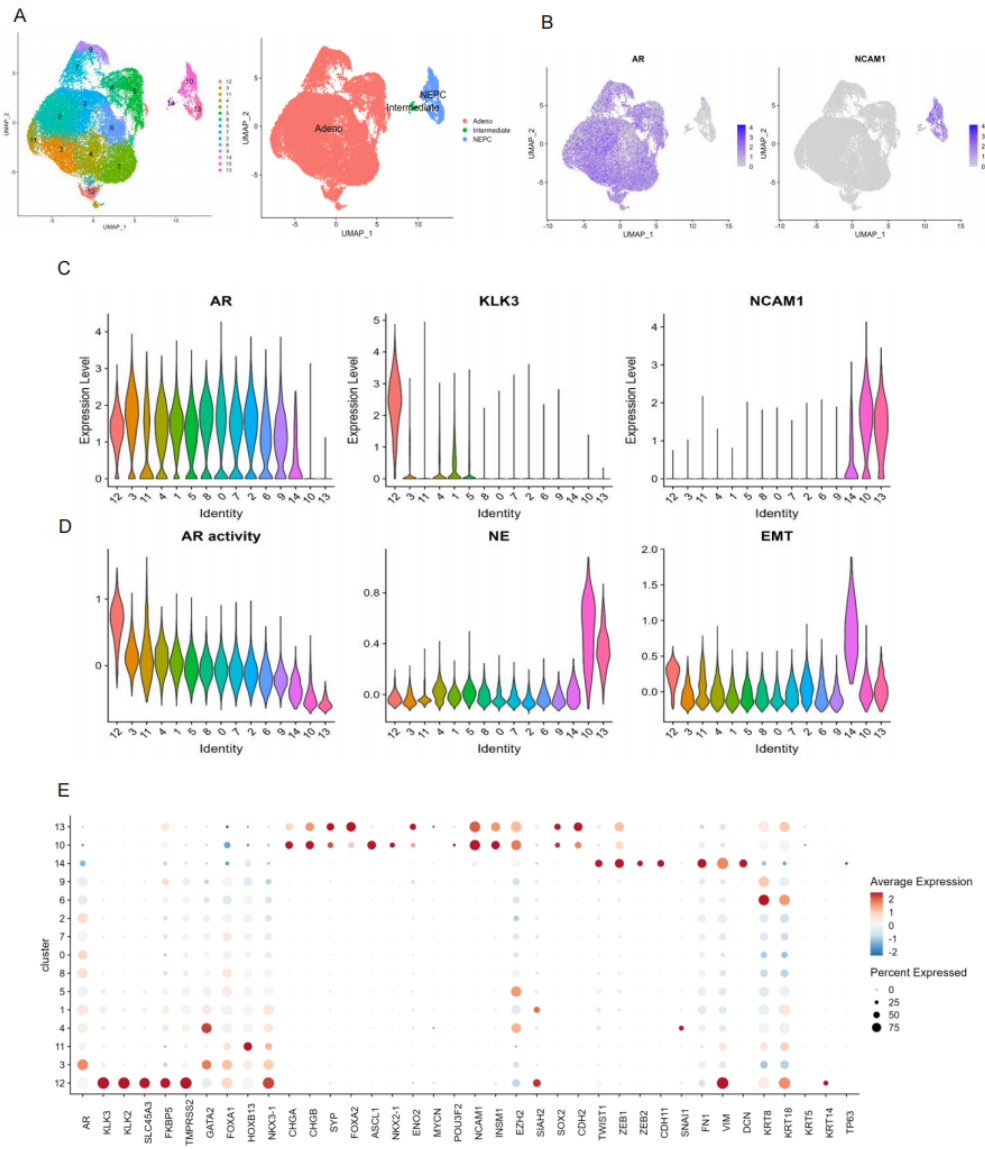


Figure 1. Single-cell transcriptomic profiling of LTL331/331R PDX during treatment-induced NEPC transdifferentiation.

- UMAP embedding of seven time-point tumor samples (from pre-castration through relapse) in the LTL331/331R PDX model. Left: Fifteen unbiased clusters (1–15) are displayed, each represented by a unique color. Right: clusters are grouped into three lineage states: AR-positive adenocarcinoma (Adeno; clusters 1–12), intermediate (cluster 14), and AR-negative NEPC (NEPC; clusters 10 and 13);
- Feature UMAPs showing single-cell expression of AR and NCAM1 (\log_2 -normalized); grey indicates no detectable expression;
- Violin plots of AR, KLK3 and NCAM1 expression levels across all fifteen clusters;
- Violin plots of lineage-program scores, i.e., AR activity, neuroendocrine (NE) score, and epithelial–mesenchymal transition (EMT) score, demonstrating high AR activity in Adeno clusters (especially pre-castration cluster 12), peak NE scores in NEPC clusters (10, 13), and high EMT in the intermediate cluster 14;
- Dot plot of selected marker genes showing mean expression (color, \log_2) and percent expressing cells (size) across clusters

Figure 2

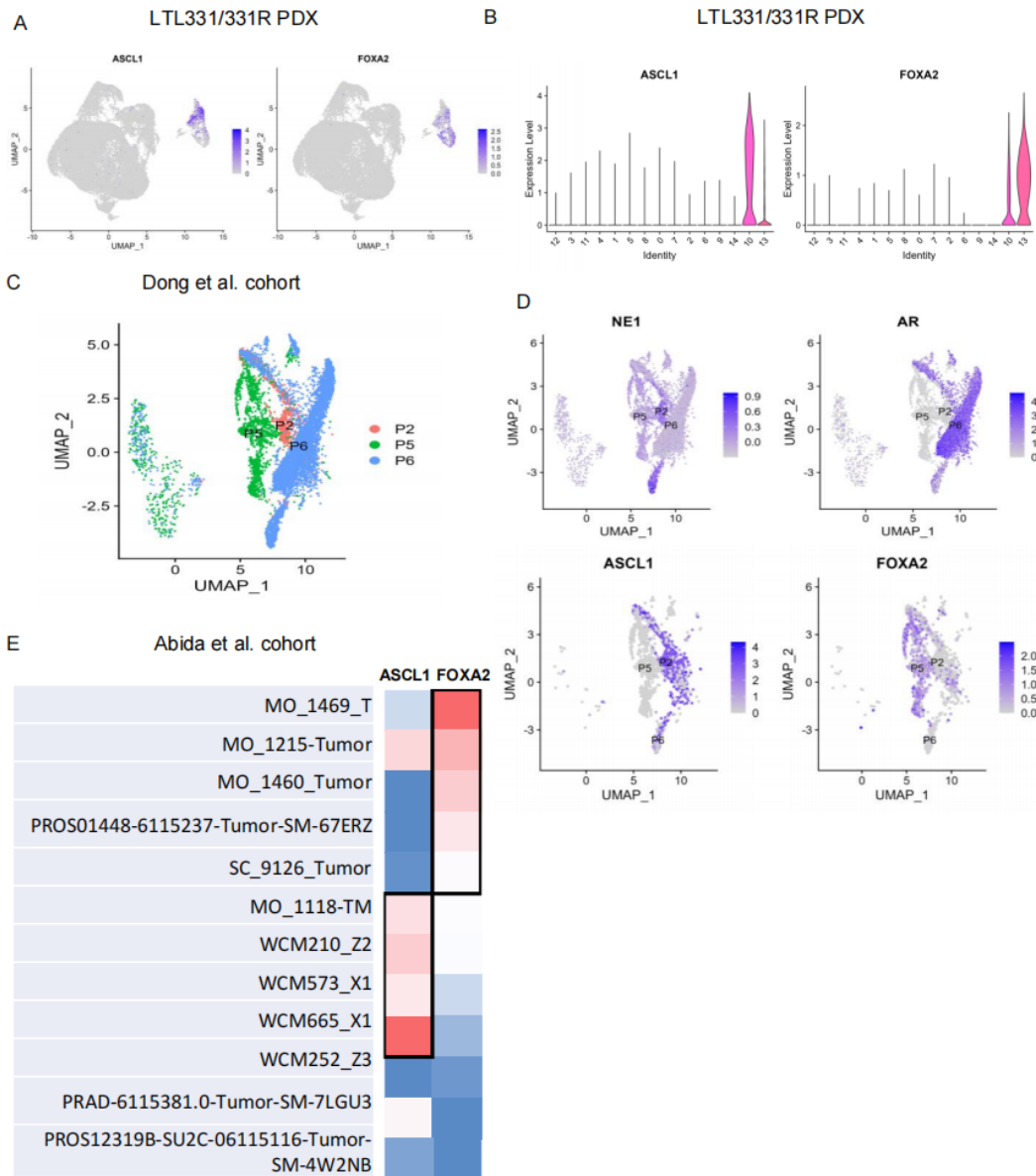


Figure 2. Two distinct NEPC subpopulations in the LTL331/331R PDX model reflect clinical heterogeneity.

- Feature UMAPs showing single-cell expression of ASCL1 and FOXA2 (\log_2 -normalized); grey indicates no detectable expression;
- Violin plots of ASCL1 and FOXA2 expression across the fifteen identity clusters; only cluster 10 exhibits high ASCL1, whereas cluster 13 shows elevated FOXA2;
- UMAP embedding of single cancer cells from three clinical NEPC patients, colored by sample (P2, P5, P6), threshold: AR- and NE score > 0;
- Feature UMAPs in the Dong et al. cohort for NE score, AR, ASCL1 and FOXA2 (\log_2 -normalized). ASCL1^{high} and FOXA2^{high} clusters mirror the PDX-derived clusters;
- Heatmap of bulk RNA-seq from AR-/NE+ NEPC clinical samples, showing inverse expression of ASCL1 and FOXA2 across 12 patients; red/blue indicates higher/lower \log_2 expression.

Figure 3

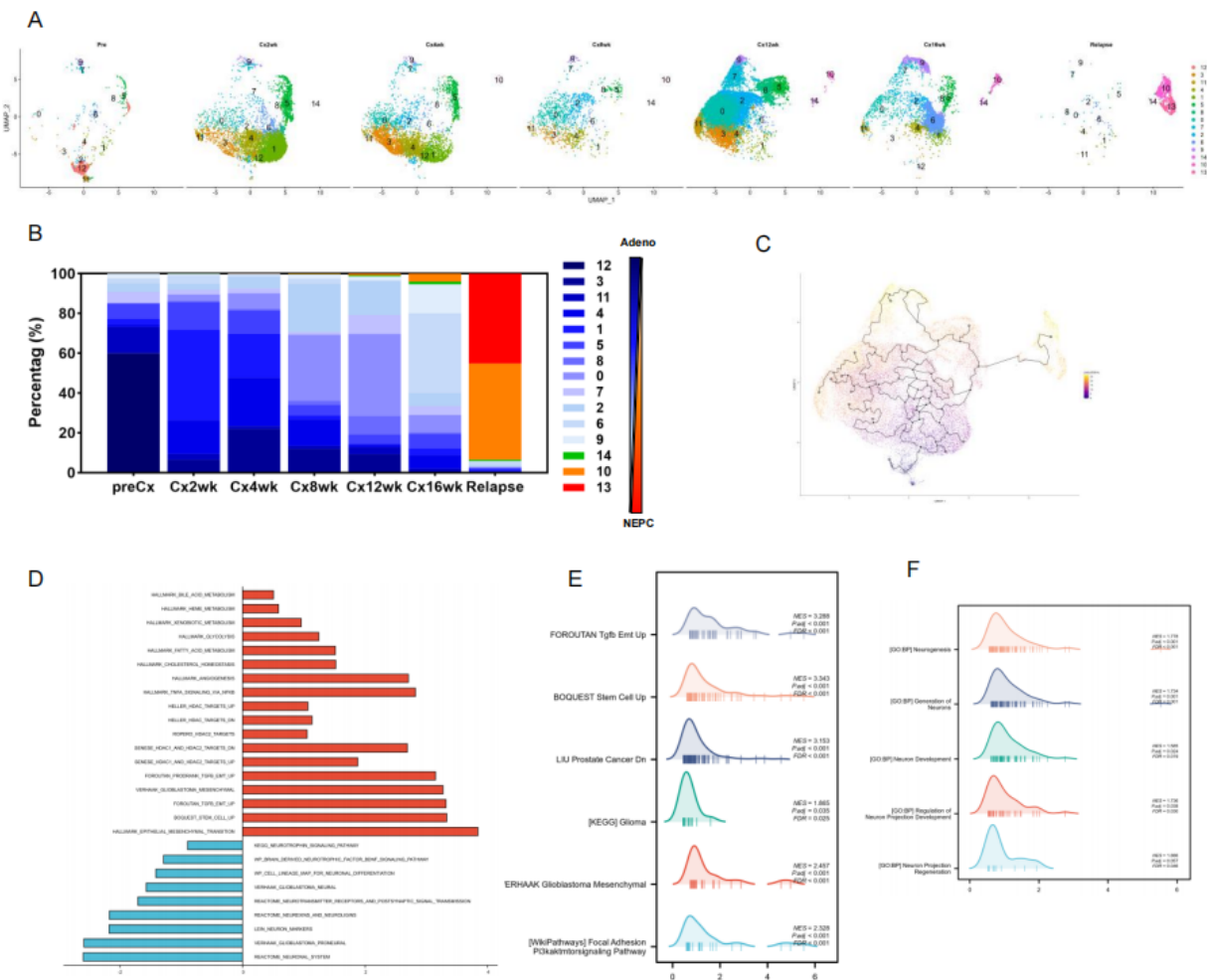


Figure 3. Longitudinal single-cell analysis identifies an intermediate cell state during NE transdifferentiation.

- UMAP projections of LTL331/331R cells at seven time points;
- Stacked bar plot showing the percentage of cells in each cluster across time points. Adeno clusters are shown in blue, the intermediate cluster 14 in green, and NEPC clusters (10 and 13) in orange and red;
- Monocle 3 trajectory analysis indicates that adenocarcinoma clusters transition through cluster 14 en route to the NEPC clusters.
- GSEA bar chart comparing intermediate cluster 14 to NEPC clusters: red bars denote pathways positively enriched in cluster 14, blue bars denote pathways negatively enriched; highlighted sets include EMT, TGF- β -driven EMT, mesenchymal/stem cell programs, metabolic pathways (bile acid, fatty acid, cholesterol homeostasis, glycolysis, xenobiotic metabolism) and HDAC regulatory signatures;
- F. Density plots comparing intermediate cluster 14 (orange) and Adeno clusters (blue), E, KEGG; F, GO.

Figure 4

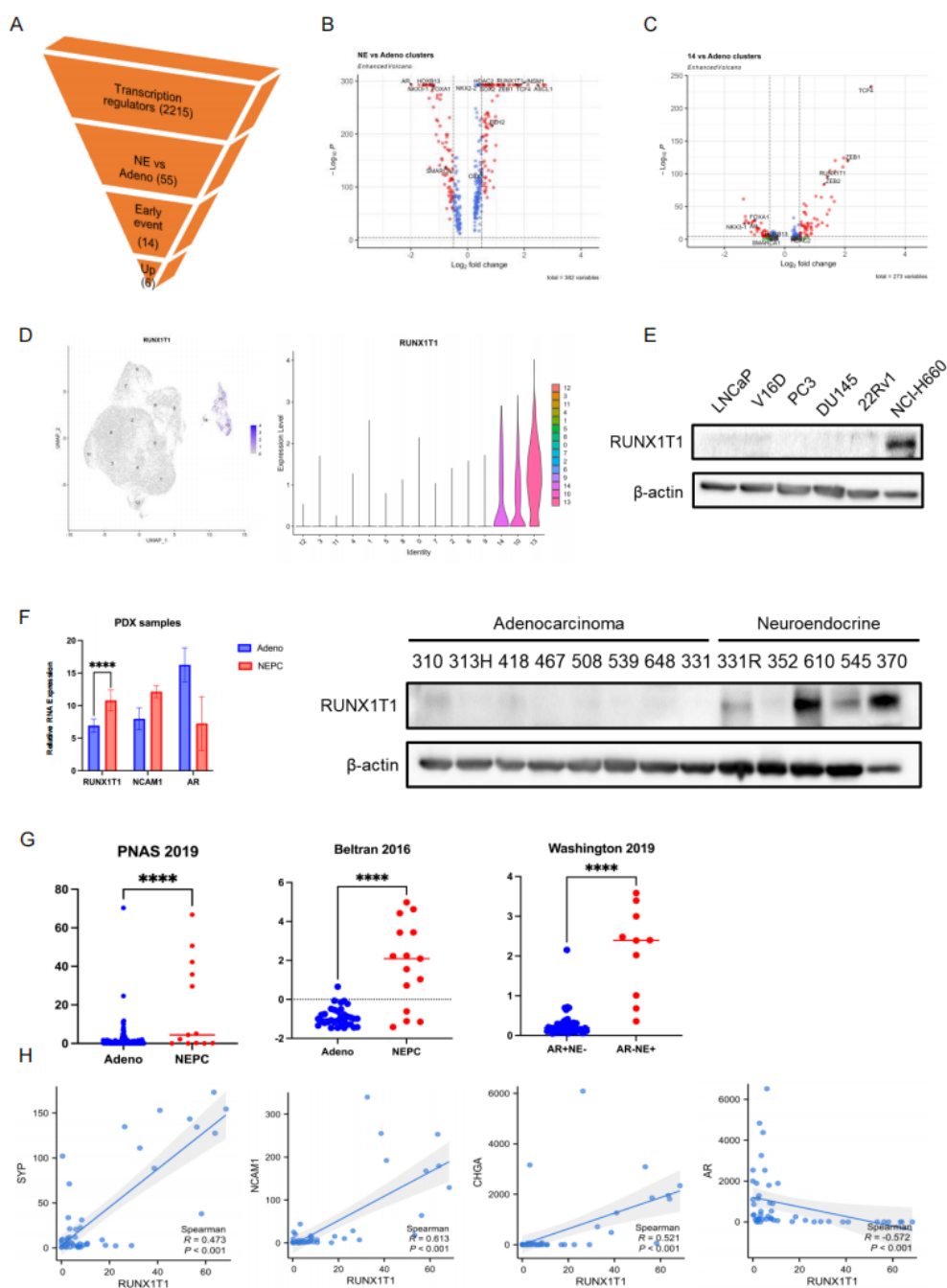


Figure 4. Identification of RUNX1T1 as a novel early driver of early NE transdifferentiation.

- Inverted funnel summarizing stepwise identification of candidate early epigenetic regulators driving NEPC development;
- Volcano plot of NEPC (clusters 10,13) vs Adeno (clusters 1–12) and intermediate cluster 14 vs Adeno clusters, fold change >2 and $p < 0.001$ are highlighted;
- Feature UMAP (left) and violin plot (right) of RUNX1T1 expression across all clusters, showing upregulation in clusters 10, 13 and 14;
- RUNX1T1 expression by western-blot in prostate cancer cell lines;
- RNA (left) and protein (right) expression of RUNX1T1 in LTL PDX samples;
- RUNX1T1 expression in bulk RNA-seq from three clinical cohorts;
- Spearman correlation of RUNX1T1 with SYP, NCAM1, CHGA and AR expression across NEPC samples.

Figure 5

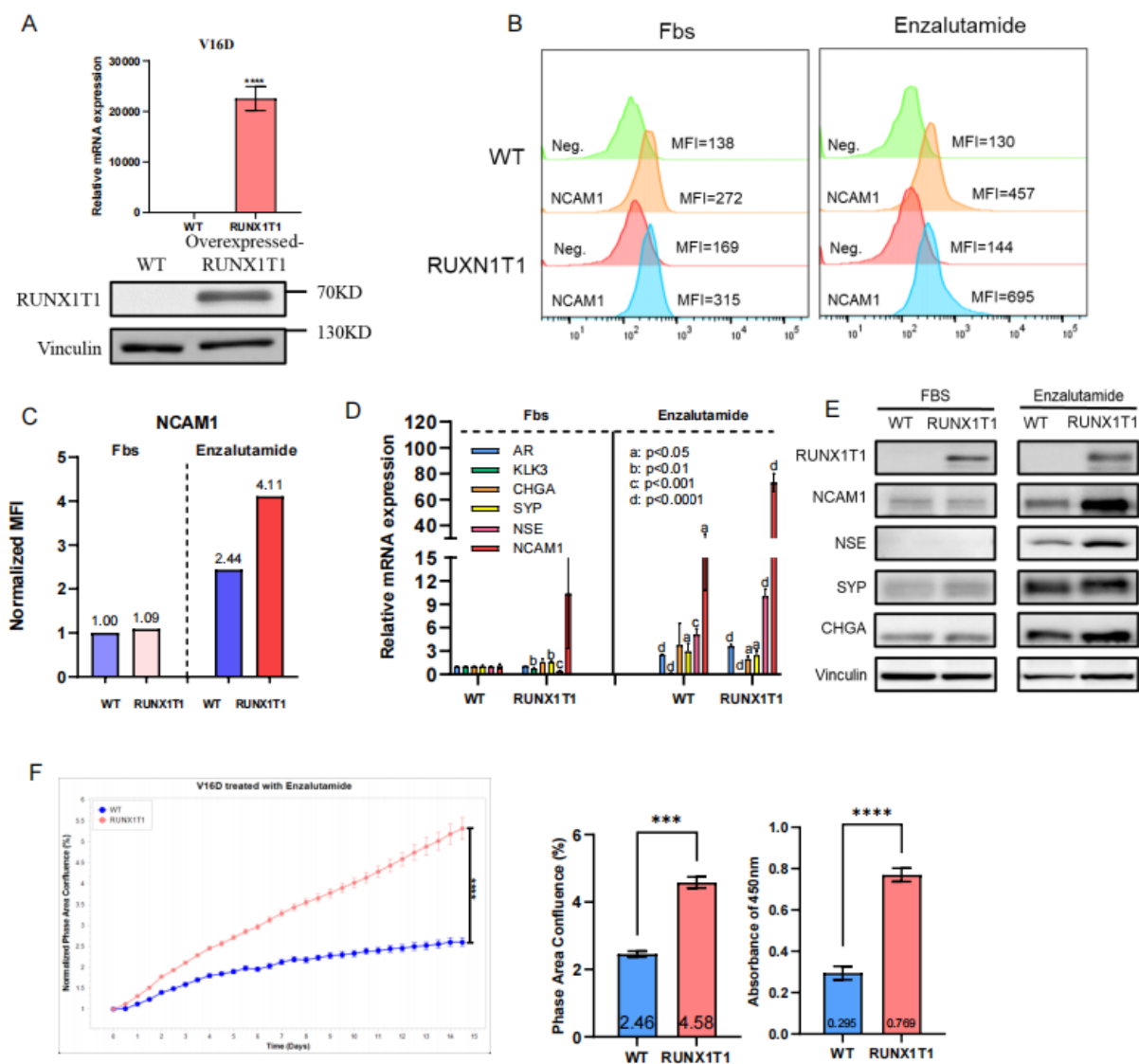


Figure 5. RUNX1T1 drives ARPI-induced NE transdifferentiation and resistance in prostate adenocarcinoma.

- qRT-PCR (top) and western blot (bottom) confirming RUNX1T1 overexpression in V16D cells, Vinculin serves as loading control;
- Flow cytometry histograms of NCAM1 in WT (green/orange) and RUNX1T1-OE (red/blue) V16D cells after 2 weeks in FBS (left) or 10 μ M enzalutamide (Enza; right). Mean fluorescence intensity (MFI) is indicated;
- Bar plot of normalized NCAM1 MFI in WT and RUNX1T1-OE cells under FBS and Enza;
- qRT-PCR of RNA expression of NE markers (CHGA, SYP, NSE, NCAM1), AR and AR target KLK3 in WT and RUNX1T1-OE cells after 2 weeks cultured with FBS or Enza;
- Western blot of RUNX1T1, NCAM1, NSE, SYP and CHGA in WT and RUNX1T1-OE V16D cells cultured in FBS or Enza; vinculin as loading control;
- RUNX1T1-OE markedly enhances the proliferation rate of V16D cells cultured in 10 μ M enzalutamide, as shown by real-time growth curves (left; WT in blue, OE in red) and by endpoint phase-area confluence and absorbance at day 15 (right; *** p < 0.001, **** p < 0.0001).

Figure 6

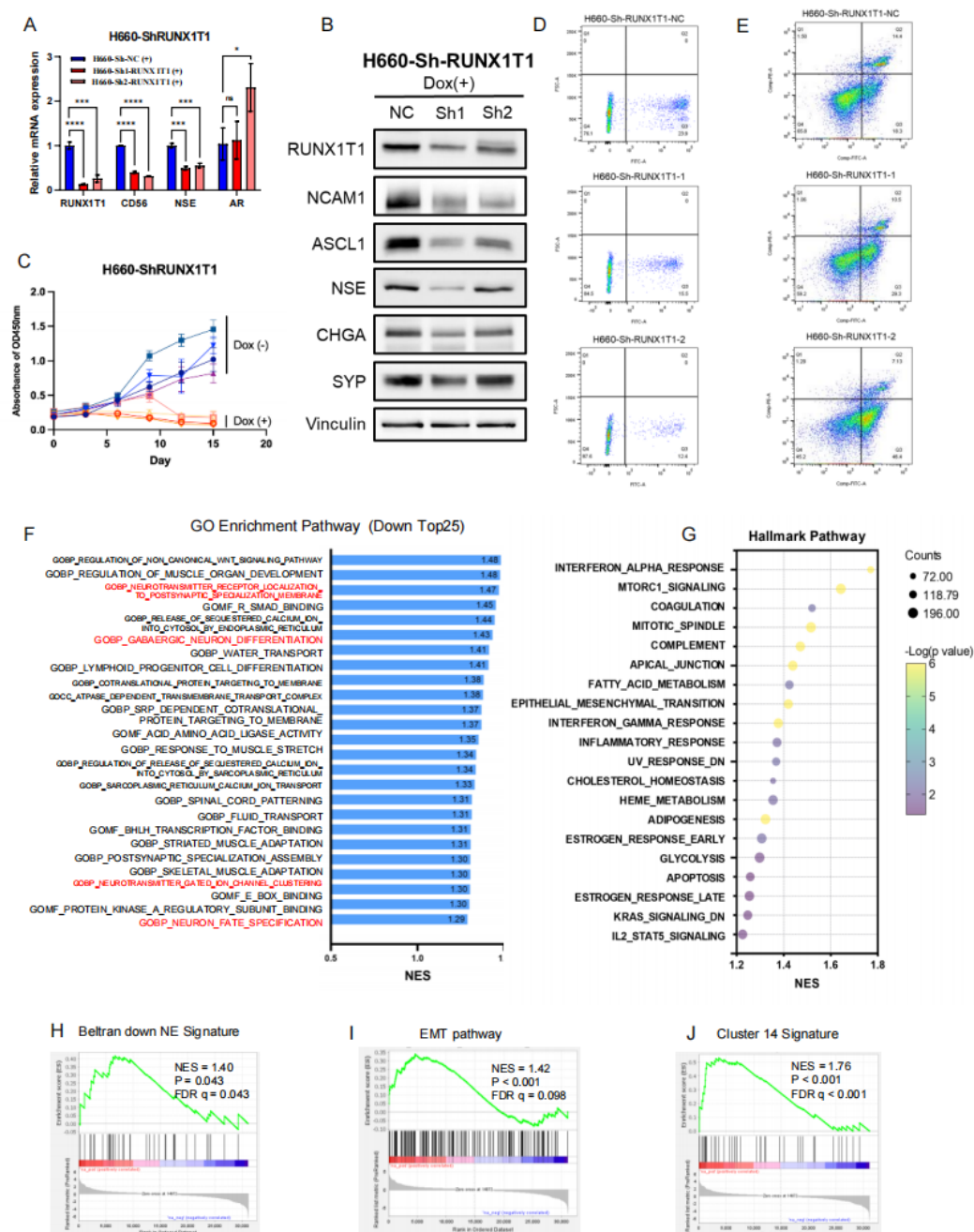


Figure 6. RUNX1T1 knockdown reverses NE phenotype and impairs NEPC cell survival.

- NA expression of RUNX1T1, NCAM1, NSE, ASCL1 and AR by qRT-PCR in H660-ShNC and two independent H660-ShRUNX1T1 lines (Sh1, Sh2) with (Dox+) or without (Dox-) doxycycline (* p < 0.05, ** p < 0.01, *** p < 0.001, **** p < 0.0001);
- Protein expression of RUNX1T1, NCAM1, ASCL1, NSE, CHGA and SYP by western blot in H660-ShNC and H660-ShRUNX1T1 cells ± doxycycline, Vinculin serves as loading control;
- Cell viability of H660-ShNC and H660-ShRUNX1T1 over 21 days with or without Dox, showing impaired proliferation upon RUNX1T1 knockdown;
- EdU assay by flow cytometry showed H660-ShRUNX1T1 cells incorporate fewer EdU+ cells (Q3) than H660-ShNC, indicating RUNX1T1 knockdown impairs H660 proliferation;
- Annexin V/PI apoptosis assay revealing increased apoptotic fraction (Q3) in H660-ShRUNX1T1 cells;

- F. GSEA bar chart of the top 25 downregulated GO pathways in H660-ShRUNX1T1 vs ShNC (NES values), highlighting loss of neuronal development programs (red);
- G. Hallmark pathway dot plot of upregulated features in H660-ShRUNX1T1 cells (dot size represents gene counts and color indicates $-\log_{10} p$);
- H. I. J. GSEA enrichment plots showing significant enrichment in H660-ShRUNX1T1 cells of the published NEPC-down signature (G), the EMT hallmark pathway (H), and the cluster 14 signature (top 50 upregulated genes; J), with NES and FDR values indicated.